Circulation and transport of water masses in the Lazarev Sea, Antarctica, during summer and winter 2006

Boris Cisewski [a,b,*], Volker H. Strass [a], Harry Leach [c]

Manuscript Draft

(05/11/2010)

[a] Alfred-Wegener-Institut für Polar- und Meeresforschung,

P.O. Box 120161, 27515 Bremerhaven, Germany

[b] Institut für Umweltphysik, Abteilung Ozeanographie, Universität Bremen

P.O. Box 330440, 28334 Bremen, Germany

[c] Department of Earth and Ocean Sciences, University of Liverpool, Liverpool, L69 3GP,

United Kingdom

[*] Corresponding author at: Alfred-Wegener-Institut für Polar- und Meeresforschung, P.O. Box 120161, 27515 Bremerhaven, Germany. Tel.: +49 471 4831 1816; fax: -471 4831 1797.
E-mail address: Boris.Cisewski@awi.de (B. Cisewski)

Abstract

The distribution and circulation of water masses in the region between 6°W and 3°E and from the Antarctic continental shelf to 60°S are described from hydrographic and shipboard acoustic Doppler current profiler (ADCP) data taken during austral summer 2005/2006 and austral winter 2006. In both seasons two gateways are apparent, where Warm Deep Water (WDW) and other water masses enter the Weddell Gyre through the Lazarev Sea: (a) a probably topographically trapped west/southwest circulation around the northwestern edge of Maud Rise with maximum velocities of about 20 cm s^{-1} and (b) the Antarctic Coastal Current, which is confined to the Antarctic continental shelf slope and is associated with maximum velocities of about 25 cm s^{-1}.

Along two meridional sections that run across the top of Maud Rise along 3°E, geostrophic velocity shears were calculated from CTD measurements and referenced to velocity profiles recorded by an ADCP in the upper 300m. The mean accuracy of the absolute geostrophic velocity is estimated at ±2 cm s^{-1}. The net baroclinic transport across the 3°E section amounts to 20 and 17 Sv westward for the summer and winter season, respectively. However, the comparison between geostrophic estimates and direct velocity measurements shows that the circulation within the study area has a strong barotropic component, i.e. that calculations based on the dynamic method underestimate the transport considerably. The net absolute volume transports across the 3°E transects result in a westward flow of 23.8 ± 19.9 Sv (austral summer) and 93.6 ± 20.1 Sv (austral winter).

1. Introduction

The Weddell Sea is an important region for the formation of Antarctic Bottom Water (AABW), which is the densest of the water masses implicated in the thermohaline circulation of the world ocean (Orsi et al., 1999). The circulation of the Weddell Sea is dominated by the, mainly wind-driven, cyclonic Weddell Gyre that controls the large-scale ocean circulation extending from the Antarctic Peninsula eastward to approximately 20°-30°E and covering both the Weddell and Enderby Basins (Deacon, 1979; Gouretski and Danilov, 1993; Orsi et al. 1993). The southern and western boundaries of the gyre are aligned with the continental margin of Antarctica and the Antarctic Peninsula. The ridge system north of 55°S, which consists of the South Scotia, North Weddell and Southwest Indian Ridge, bounds the Weddell-Enderby Abyssal Plain to the north (Fig.1a). The northern limb of the Weddell Gyre is dominated by easterly flow that joins the Antarctic Circumpolar Current (ACC). The broad easternmost limb of the Weddell Gyre between about longitudes 10°W and 40°E, where the ACC is deflected southward, is where Circumpolar Deep Water (CDW), locally called Warm Deep Water (WDW), enters the Weddell Gyre (Deacon, 1979; Bagriantsev et al., 1989; Gouretski and Danilov, 1993; Orsi et al., 1993; Schröder and Fahrbach, 1999) through the Lazarev Sea. On its course through the eastern limb this deep water mass is raised from about 1000 m depth in the ACC to about 400 m depth in the Lazarev Sea due to Ekman suction in the Antarctic Divergence.

A striking bathymetric feature of the Lazarev Sea is the Maud Rise seamount, which rises from the relatively flat surrounding abyssal plain at a depth of greater than 5000 m upward to within 1600 m of the sea surface. The horizontal distribution of the temperature maximum indicates an anticyclonic circulation of anomalously warm WDW over the northern and western flanks of Maud Rise (Bersch et. al., 1992; Gordon and Huber, 1995; Muench et al., 2001; La Steur et al., 2007), which surrounds the seamount as a “Halo” (Gordon and Huber,

1990; Muench et al., 2001), whereas an isolated Taylor column of colder and less saline water overlies the top of the rise. Isolated spots of WDW pass along the northern flank of Maud Rise and contribute to quasi-stationary pools of WDW west of it (Bersch et al., 1992; Gordon and Huber, 1995). These warm pools lead to large upward heat fluxes and a consequent loss of pack ice (McPhee et al., 1996; Muench et al., 2001; Sirevaag et al., 2010). The upwelled WDW, which is the remnant of the regional CDW, is transported farther to the west-southwest by the southern limb of the Weddell gyre, where it is modified by atmosphere-ice-ocean interaction and mixes with both fresh and cold Winter Water and cold High Salinity Shelf Water. Eventually, all three water masses mix near the shelf edge (Foster and Carmack, 1976) and become newly formed Weddell Sea Deep Water or Weddell Sea Bottom Water, a precursor of the Antarctic Bottom Water.

Although the large-scale circulation of the Weddell-Gyre is well known from the distribution of various water mass characteristics (e.g. Deacon, 1979; Gouretski and Danilov, 1986; Orsi et al., 1993; Fahrbach et al., 1994), a lack of knowledge concerning absolute velocities, their temporal variability and spatial structures, even in the southeastern limb still exists. Previous estimates of the Weddell Gyre transport varied from 17 Sv (Whitworth and Nowlin, 1987) to 97 Sv (Carmack and Foster, 1975) depending on the chosen method.

The main purpose of this paper is the investigation of the hydrographic structure, circulation and transport of the main water masses of the southern limb of the Weddell Gyre in the eastern inflow region of the Weddell Sea. In this study, we present the results of two hydrographic surveys, performed during austral summer 2005/2006 and austral winter 2006 as part of the Lazarev Sea Krill Study (LAKRIS). These surveys cover the area between 6°W and 3°E and from the Antarctic continental shelf to 60°S. The combination of conductivity-temperature-depth (CTD) profile data and ship-mounted acoustic Doppler current profiler (ADCP) measurements was used to obtain a quasi-synoptic picture of the water mass

distribution and circulation of the study area. The ADCP measurements provide measurements of the velocity field on scales normally not resolved by hydrographic stations and mooring locations and were used as an absolute reference for geostrophic current and transport estimations.

2. Data and methods

2.1 CTD profiler

Between November 2005 and August 2006, two hydrographic cruises were conducted in the southeastern Weddell Sea aboard the R.V. *Polarstern* as part of the extensive field campaign of the Lazarev Sea Krill Study (LAKRIS), dedicated to identifying relationships between the physical environment and the abundance of zooplankton and especially krill. In total, 177 casts with a CTD type Sea-Bird Electronics SBE 911plus were made during both LAKRIS surveys, in order to map the hydrographic field of the study area (Table 1). Of these, 82 extended to full ocean depth, while the others were limited mostly to the upper 1,000 m of the water column. All CTD stations were organized in a regular grid, made up of four meridional sections running between 60°S and 70°S and along 3°E, 0°E, 3°W and 6°W during the summer cruise (Fig. 1b). The entire transect along 6°W of the planned grid had to be cancelled due to heavy ice conditions during the following winter survey (Fig. 1c). The distance between stations along the meridional sections was nominally 30 nm. Water samples were collected with a Sea-Bird Carousel sampler with 24 12-l bottles. For in situ calibration, temperatures were measured with a digital thermometer Sea-Bird SBE35, and salinity samples were analyzed with a Guildline-Autosal-8400A salinometer onboard. The temperature sensor was calibrated at the manufacturer a few months prior to the cruise and

afterwards to an accuracy better than 0.001°C for both surveys. Salinity derived from the CTD measurements was calibrated to a final accuracy of better than 0.002 for both cruises by comparison to the salinity samples.

2.2 Vessel-mounted acoustic Doppler current profiler

Vertical profiles of ocean currents down to 335 m depth were measured on board R. V. *Polarstern* continuously using a hull-mounted acoustic Doppler current profiler (Ocean Surveyor; Teledyne RD Instruments USA, Poway, California, 150 kHz nominal frequency). The transducers were located 11 m below the water line and were protected against ice floes by an acoustically transparent plastic window. The velocity components *U* (eastward), *V* (northward) and *W* (upward) were averaged in 2min ensembles in 4m thick depth bins between 19 and 335 m depth. The reference layer was set to bins 6 to 15, avoiding near surface effects and biases near bin 1. Heading, roll and pitch data from the ship's gyro platforms were used to convert the ADCP velocities into earth coordinates. The ship's velocity was calculated from position fixes obtained by the Global Positioning System (GPS) or DGPS if available. Accuracy of the ADCP velocities depends mainly on the quality of the position fixes and the ship's heading data. Further errors stem from a misalignment of the transducer with the ship's centerline. To reduce these errors, standard watertrack calibration methods (Joyce, 1989; Pollard and Read, 1989) were applied to provide a velocity scale factor and a constant angular offset between the transducer and the length axis of the ship. Further ADCP processing was done by using the CODAS3 software package developed by E. Firing and colleagues (Firing, 1991). Barotropic tidal currents were predicted and removed using the Circum-Antarctic Tide Model CATS02.01 developed by Padman et al. (2002).

2.3 Deriving absolute velocities

The average geostrophic current v_g referenced to a velocity v_{ref} on a certain isobaric surface between two CTD stations *A* and *B* was calculated as follows

$$v_g = \frac{1}{fL}\left(\Delta D_B - \Delta D_A\right) + v_{ref} \quad (1)$$

where (ΔD_B-ΔD_A) is the difference in dynamic height, calculated from integrating over pressure the specific volume anomalies at stations, *B* and *A*, separated by distance *L*, and *f* is the coriolis parameter. However, the difficulty inherent to the dynamic method, even if the density and the station locations are very well determined, is that the reference velocity is unknown and must be determined by other means. To overcome this problem, we used the referencing method presented by Pickart and Lindstrom (1994) and Cokelet et al. (1996) and combined the ADCP data with the baroclinic geostrophic currents derived from the hydrographic measurements. To obtain the ADCP-referenced geostrophy, the normal component of the ADCP currents after prior correction for tidal motion was spatially averaged between the CTD casts. This provided mean ADCP velocity profiles for the same horizontal spacing for which also the baroclinic geostrophic profiles were calculated. The baroclinic geostrophic velocities, which were always calculated relative to the deepest common level between neighboring station pairs, were adjusted to fit the normal ADCP velocity component for a specified depth range. For each pair of ADCP and baroclinic geostrophic profiles that depth range was selected as that where the shears matched best and so, the averaged offset reveals only a small standard deviation. The depth range varied from profile to profile between 45 m (minimum) to 301 m (maximum), to avoid effects both from surface forcing and weak signals close to the range limit. The offset between the mean ADCP and the baroclinic geostrophic current component in the depth range of best-matching shears then constitutes the barotropic current component. The absolute current component then is obtained by adding the baroclinic and barotropic components. The spatial resolution of the

derived absolute velocity field was 4 m in the vertical and 55 km horizontally, the latter being determined by the station distances.

Averaging of the ADCP data also helps to reduce the measurement uncertainty of single-ping ADCP measurements to acceptable levels. The manufacturer (Teledyne RDI) indicates a single-ping uncertainty of ±30 cm s^{-1} for the 150 kHz Ocean surveyor configured in longrange mode with a bin length of 4 m. The statistical uncertainty of the velocity measurements reduces to standard errors of ±5 cm s^{-1} $\left(30/\left(\sqrt{37}\right)\text{cm s}^{-1}\right)$ if we average over 37 single pings, which corresponds to the theoretical precision of u and v averaged over 2 minutes. In this study, about 100 individual ADCP ensembles made up a typical 55-km long section between a CTD pair. This implies an error in the section-averaged ADCP reference velocity of ±0.5 cm s^{-1} $\left(30/\left(\sqrt{37}\cdot\sqrt{100}\right)\text{cm s}^{-1}\right)$.

2.4 Error estimation for geostrophic referencing

Errors in the calculation of the geostrophic velocity dv_g include uncertainties in the station spacing dL, uncertainties in the dynamic height anomaly $d\Delta D$, and uncertainties in the reference velocity dv_{ref} (see Johns et al., 1989).

$$dv_g = \sqrt{\left(\frac{d\Delta D}{f\,L}\right)^2 + \left(\frac{dL}{L}v_g\right)^2 + \left(dv_{ref}\right)^2} \quad (2)$$

The estimated error in dynamic height, $d\Delta D$, can be calculated from the estimated error in the specific volume anomaly $d\delta$, which depends on the measurement errors in temperature, salinity and pressure ($\Delta T = 0.001$°C, $\Delta S = 0.002$, $\Delta p = 1 \times 10^4$ Pa).

$$d\delta = \left(\frac{\partial\delta}{\partial T}\right)\cdot dT + \left(\frac{\partial\delta}{\partial S}\right)\cdot dS + \left(\frac{\partial\delta}{\partial p}\right)\cdot dp \quad (3)$$

The partial derivative of δ with respect to pressure is neglected because it does not contribute to the horizontal gradients in $d\Delta D$ along isobaric surfaces. The partial derivatives were estimated using variations of a typical mean *T-S* profile within the Lazarev Sea

$$\frac{\partial \delta}{\partial T} = 5.6 \times 10^{-7}\ \mathrm{m^3 kg^{-1}}$$

$$\frac{\partial \delta}{\partial S} = 2.9 \times 10^{-7}\ \mathrm{m^3 kg^{-1}}$$

$$d\delta = \sqrt{\left(\frac{\partial \delta}{\partial T} \cdot dT\right)^2 + \left(\frac{\partial \delta}{\partial S} \cdot dS\right)^2} = 8.1 \cdot 10^{-10}\ \mathrm{m^3 kg^{-1}} \qquad (4)$$

These variations lead to an ultimate error of approximately 0.045 $m^2\ s^{-1}$ between the surface and the 5500-dbar isobar.

$$d\Delta D = d\delta\, dp = 0.045\ \mathrm{m^2 s^{-2}} \qquad (5)$$

Thus, the dynamic height component of the velocity error is $dv_g = d\Delta D / fL$ = 0.045 $m^2 s^{-2}$ / ($1.3e^{-4}\ s^{-1}$ × 55560 m) = 0.6 cm s^{-1}.

The second error in geostrophic velocity arises from the uncertainties in station spacing. The maximum position uncertainty for each CTD station was ± 50 m, leading to an error of

$$dL = \sqrt{50^2 + 50^2} = \pm 71\mathrm{m}. \qquad (6)$$

The velocity error due to inaccuracy in determining the station spacing is $dv_g = dL / L \times v_g$ = (71 m / 55560 m) × 0.1 m s^{-1} = 0.01 cm s^{-1}.

The third error in geostrophic velocity arises from the uncertainties in the reference velocity dv_{ref}. Errors in the ADCP reference velocity derive mainly from two sources: instrument error and ageostrophic motion including Ekman drift currents, tides, internal waves or inertial oscillations. Thus, tides were removed from the ADCP velocities using the CATS02.01 Tide Model (Padman et al., 2002). To analyze, whether the wind field has an effect on the referenced velocity or not we estimated the Ekman depth D_E after Pond and Pickard (1983), where W is the wind speed, which was measured aboard R.V. Polarstern, and ϕ is the geographical latitude.

$$D_E = \frac{4.3W}{\sqrt{(\sin|\phi|)}} \quad (7)$$

The Ekman depth varied between 19.8 and 80.2 m during the summer survey and between 14.2 and 69.3 m during the winter survey, well above the chosen reference layer to avoid effects from wind forcing. We assume the accuracy of the ageostrophic velocities to be of the order of 2 cm s^{-1}, taking the described sources of errors into consideration. Adding their variances to the instrument error estimated as 0.5 cm s^{-1}, the square root of the sum yields a net reference layer standard deviation of about 2 cm s^{-1}. While the uncertainties in station spacing and in dynamic height anomaly are of minor importance for the estimated error in the geostrophic calculation (< 1 cm s^{-1}), the major error in the ADCP reference velocity derive from ageostrophic motion. Following equation (2) this leads to a mean accuracy of the absolute geostrophic velocity $dv_g = \sqrt{(0.6\ \mathrm{cms}^{-1})^2 + (0.01\ \mathrm{cm\,s}^{-1})^2 + (2\ \mathrm{cm\,s}^{-1})^2} = 2\ \mathrm{cm\,s}^{-1}$.

3. Results

3.1 Hydrographic structure

The water of the Lazarev Sea observed in this study is classified into four major water masses according to their potential temperature (Θ) and salinity (S) characteristics (Fig. 2, Table 2). In our nomenclature we follow mostly the definitions of Carmack and Foster (1975). Hydrographic conditions in the study area during austral summer 2005/2006 and austral winter 2006 are illustrated by two meridional sections along 3°E from 60°S to 70°S (Figs. 3 and 4).

The open ocean surface layer consists mainly of less saline and (near)-freezing-point Antarctic Surface Water (AASW). During the austral summer, after the sea ice receded, the

Winter Water (WW) is overlain by a shallow layer of low-salinity and slightly warmed meltwater. The mean mixed layer depth (MLD) was estimated at 25 ± 9m using the mixed layer criterion introduced by Cisewski et al. (2005, 2008). Underneath the AASW the Warm Deep Water (WDW) is found, which is the warmest water mass observed in the study area and is defined by potential temperatures $\theta > 0$°C. The maximum temperature of the WDW is accompanied by a salinity maximum of about 34.7. Whereas the northern slope of Maud Rise is overlain by a pronounced warm WDW core (T_{Max} = 1.16°C), the maximum temperature is much lower over the top of Maud Rise (T_{Max} = 0.42°C). Between the southern flank of the seamount and 68°S T_{Max} gradually increases from 0.6°C to 0.76°C. A second isolated core of warm WDW with a temperature maximum of 0.97°C is found near the continental slope at 68.5°S. At 69°S the surface layer deepens from 120 m towards the shelf break to more than 600 m near the Antarctic Slope Front, which separates the Winter Water and the Warm Deep Water from the colder and less saline Shelf Waters near the Antarctic continent. The cold water mass underneath the WDW with potential temperatures between 0°C and -0.7°C is the Weddell Sea Deep Water (WSDW). Only north of Maud Rise, Weddell Sea Bottom Water (WSBW) with potential temperature below -0.7°C is found at the sea floor.

During the austral winter, the mixed layer forms a nearly homogeneous layer of Winter Water (WW), which represents the (near)-freezing-point type of AASW with an average thickness of 108 ± 26m between 60° and 69°S (Fig. 4). Further south, the MLD deepens from 80 to 453 m between the ASF and the continental shelf. However, it is remarkable that the WDW layer reveals almost similar patterns as observed during the foregoing summer (Fig. 3). The northern slope of Maud Rise is overlain by a warm WDW core (θ_{Max} = 1.16°C). At this station the WDW is uplifted into the upper 100 meter. A second isolated core of warm WDW with a maximum potential temperature of 0.97°C is found near the continental slope at 68.5°S.

3.2 Circulation and Transports

3.2.1 Direct measurements

Fig. 5a illustrates the tide-corrected horizontal currents in the depth range 150 – 200 m measured with the VM-ADCP and averaged 5 km alongtrack for the summer survey. The vectors show the highest velocities within the westward flowing Antarctic Coastal Current (AntCC), which is confined to the Antarctic continental shelf slope and is associated with maximum velocities of about 21-42 cm s^{-1}, and a west/southwest circulation around the northern and northwestern flanks of Maud Rise with maximum velocities of about 20-23 cm s^{-1}, respectively. This jet is 30 to 50 km wide and follows the 4000 m- and 5000 m-isobaths, which locally correspond to the deepest part of the slope of the seamount and the continental slope. However, just south of this jet, recirculation occurs in a narrow band with maximum velocities of about ~15 cm s^{-1}. Over the top of Maud Rise the velocities are small. At the two westernmost transects the velocity field is dominated by a number of mesoscale features indicative of eddies and meanders.

Fig. 5b shows the streamfunction based on the tide-corrected ADCP data, which are vertically averaged between 150 – 200 m and temporarily averaged for periods of hydrographic station work. The two most striking features are two strong jets, one between 63° and 64°S, over the northern flank of Maud Rise, and another between 69° and 70°S, close to the continental shelf slope. The streamfunction reveal a west/southwest circulation around the northwestern edge of Maud Rise with maximum velocities of about 8 cm s^{-1} and the AntCC following the Antarctic continental shelf, which is associated with maximum velocities of about 20 cm s^{-1}. The horizontal distribution of the *T*max temperature agrees well with this circulation pattern (Fig. 5c) and suggests that WDW enters thorough the Lazarev Sea via the Maud Rise Jet and the offshore part of the AntCC. Warmest WDW pass along the

northern flank of Maud Rise and forms a pool immediately to the west, as far as 6°W. A second, isolated, pool is apparent at 62°S, 3°W. The second gateway of WDW is the westward flowing AntCC between 69°S and 70°S.

Fig. 6a illustrates the tide-corrected horizontal currents in the depth range 150 – 200 m measured with the VM-ADCP and averaged 5 km alongtrack for the winter survey. The entire transect along 6°W and the southernmost stations along the 0°E and 3°E transects had to be cancelled due to heavy ice conditions. Unfortunately, there is a gap in the ADCP data due to a failure in the ships navigational device along the 3°E transect between 63.5°S and 64°S, which corresponds to major parts of the northern gateway of WDW. The vectors along the 3°E transect reveal the highest velocities within the AntCC of about 34 cm s^{-1}. The streamfunction also reveals the two strong jets over the northern flank of Maud Rise and close to the continental shelf slope (Fig. 6b). However, the northern jet splits off into two branches at about 64°S, 0°E. While the northern branch flows in northwesterly direction, the southern branch flows southwestward. Interestingly, Fig. 6c shows a discontinuity of the T_{Max}-distribution around the northwestern edge of Maud Rise.

3.2.2 Baroclinic current and transport

The baroclinic velocities perpendicular to the 3°E section (Fig. 7), calculated relative to the deepest common levels of neighboring station pairs by the geostrophic methods reveal highest velocities within the westward flowing AntCC with maximum baroclinic velocities of about 6 cm s^{-1} (summer) and 10 cm s^{-1} (winter), and a westward flowing jet over the northern slope of Maud Rise with maximum velocities of about 10 cm s^{-1} (summer) and 7 cm s^{-1} (winter). Recirculation occurs in a small stream band just south of the Maud Rise Jet. Elsewhere, the baroclinic velocities are rather weak. The net baroclinic transport across the 3°E section amounts to 20.1 and 17.0 Sv eastward for the summer and winter season, respectively (Table

3 and 4). The major contributions to the total baroclinic transport stem from the Maud Rise Jet, which is located between 63°S and 63.5°S and accounts for 13.0 Sv and 7.9 Sv, and from the AntCC between 69°S and 70°S, which accounts for 2.3 and 3.1 Sv during the summer and the winter survey, respectively.

3.2.3 ADCP-referenced geostrophic current and transport

Prior to adjustment, the baroclinic currents were referenced to the deepest common levels of neighboring station pairs. The magnitude of the adjustments from relative to absolute velocities along the 3°E transect range from -7.5 to 2.1 cm s^{-1} for the summer survey. Thus, the ADCP-referenced geostrophic current is usually stronger than the relative current. Due to the high barotropic currents, the ADCP-referenced geostrophic flow field is essentially columnar and does not show a level of no motion (Fig. 8a) in major parts of the section. The current field reveals several branches with alternating eastward and westward components. Strong westward flow of about 10 cm s^{-1} occurs in a 110 km wide jet above the northern slope of Maud Rise between 63° and 64°S and above the Antarctic continental shelf between 69° and 70°S. Relatively weak eastward flows of about 1-3 cm s^{-1} occur between 60°S and 61.5°S, likely related to the northern eastward limb of the Weddell Gyre, and between 64° and 68°S, above the top of Maud Rise and its southern more gradual topographic slope.

The meridional distribution of the ADCP-referenced geostrophic volume transports across the 3°E section is shown in Fig. 9b and in the third column of Table 3 with corresponding estimates of the accuracy. The Maud Rise Jet (63° to 64°S) and the AntCC (69° to 70°S) provide the major contributions to the net transport of about -23.8 ± 19.9 Sv westward. This transport can be split into the four major water masses mentioned in Table 1. The total transport across 3°E consists of -3.9 ± 1.0 Sv (17%) AASW, -11.3 ± 6.6 Sv (46%) WDW, -8.4 ± 10.5 Sv (37%) WSDW and -0.2 ± 3.8 Sv (0%) WSBW (Table 3, Fig. 9).

Six months later the ADCP-referenced geostrophic flow field reveals also a columnar structure without any clear level of no motion (Fig. 8b). However, strong westward velocities cover a wider portion of the transect than in summer and result into a total transport of -93.6 ± 20.1 Sv. The magnitude of the adjustments from relative to absolute velocities along the 3°E transects range from -15.4 to 2.5 cm s^{-1}. The highest velocities of about 10 cm s^{-1} and 25 cm s^{-1} are found within the Maud Rise Jet and the AntCC. The total transport across 3°E during austral winter consists of -9.9 ± 1.0 Sv (11%) AASW, -30.7 ± 6.8 Sv (33%) WDW, -42.8 ± 10.6 Sv (46%) WSDW and -10.2 ± 3.8 Sv (11%) WSBW (Table 4, Fig. 10).

4. Discussion

Two hydrographic surveys performed during austral summer 2005/2006 and austral winter 2006, which cover the southern limb of the Weddell Gyre in the Lazarev Sea were used to derive an approximately synoptic picture of the hydrographic structure, circulation, and transports of the study area. The distribution of water masses of each of the meridional transects suggests that two gateways are apparent where warm deep water masses enter through the Lazarev Sea. WDW enters the study area at 63.5°S and flows within a topographically trapped west/southwest jet around the northwestern edge of Maud Rise with maximum velocities of about 21-23 cm s^{-1}, which corroborate the results of De Steur et al. (2007) who observed strong subsurface velocities up to 20 cm s^{-1} above the northern flank of the rise during the 2005 MaudNESS winter field campaign. Anomalously warm WDW cores (T_{Max} = 1°C) travel along the northern and western slope and contribute to a huge warm pool west of Maud Rise. Our results are in general agreement with previously reported hydrographic studies, e.g. those of Gordon and Huber (1995) and Bersch et al. (1992), who discussed the bathymetric effects of the Maud Rise on the stratification and circulation of the

Weddell Gyre and showed a quasi-stationary pool of relatively warm WDW immediately west of this seamount, which entered this region along the northern slope of Maud Rise.

At the two westernmost meridional transects several branches with nonnegligible near-surface velocities are associated with alternating eastward and westward components, indicating the existence of mesoscale eddy activity there. This leads to the assumption that the observed WDW cores probably shed as eddies from the western flank of Maud Rise. This is corroborated by the studies of Bersch et al. (1992) and De Steur et al. (2007). Based on current meter data, Bersch et al. (1992) observed an anticyclone of WDW, which had cut off from the main body of WDW in the lee Maud Rise. In a recent study De Steur et al. (2007) used a isopycnic ocean model, which shows that eddies of alternating sign are formed from instability of jet-like flow structure, and are subsequently shed from the western flanks of the Rise.

Our study shows that WDW also enters the study area via the offshore part of Antarctic Coastal Current. The Antarctic Slope Front (ASF), which is located around 69°S at 3°E, defines the boundary between the cold, relatively fresh waters filling the Antarctic continental shelf and the warmer, more saline waters farther offshore (Jacobs, 1991). Owing to strong horizontal density gradients, the ASF is associated with a strong baroclinic, westward transport. However, the intercomparison between geostrophic and direct velocity measurements confirm in agreement with Nunez-Riboni and Fahrbach (2009) that the AntCC also has a strong barotropic transport component.

Earlier estimates of the Weddell Gyre transports have varied between 17 Sv (Whitworth and Nowlin, 1987) and 97 Sv (Carmack and Foster, 1975) depending on the chosen method. In the absence of direct measurements Whitworth and Nowlin (1987) estimated a Weddell Gyre transport of 17.2 Sv relative to the deepest common depth between station pairs for the Greenwich Meridian section, which was in perfect agreement to the overall relative westward

transport of 17.3 Sv in the southern limb estimated by Klatt et al. (2005). In our study, the net geostrophic transport referenced to the deepest common depth of neighboring station pairs across 3°E was 20.1 Sv during the summer survey and 17.0 Sv during the winter survey, and agrees well with the estimates of Whitworth and Nowlin (1987) and Klatt et al. (2005).

However, the comparison between geostrophic and direct velocity measurements confirm in agreement with Gordon et al. (1981) and Fahrbach et al. (1991) that all currents within the study area have a significant barotropic component so that calculations based on the dynamic method underestimate the transport considerably. First indications for considerable barotropic components in the Weddell Gyre circulation resulted from the study of Carmack and Foster (1975). They used geostrophic calculations adjusted to direct current measurements and estimated a transport of 97 Sv. Gordon et al. (1981) calculated 76 Sv for the Sverdrup transport in the Weddell-Enderby Basin. Schröder and Fahrbach (1999) estimated on the basis of a combined CTD/ADCP data set an eastward transport of 61 Sv and a westward return flow of 66 Sv in the southern limb of the Weddell Gyre across the Greenwich Meridian. Beckmann et al. (1999) used a circumpolar model to investigate the wind-driven and thermohaline circulation of Weddell Gyre and yielded a pronounced and persistent double-cell structure of the Weddell Gyre with a maximum transport of ~60 Sv, in agreement with the observation of Schröder and Fahrbach (1999). Klatt et al. (2005) used current-meter observation from instruments moored from 1996 to 2001 and estimated a record length mean volume transport of 46 Sv to the east within the northern and 56 Sv to the west within the southern limb of the Weddell Gyre.

In our study, the net absolute volume transports across the 3°E transects result in an westward flow of 23.8 ± 19.9 Sv (austral summer) and 93.6 ± 20.1 Sv (austral winter), which is quite similar to the range of the previous estimates mentioned above. While the combination of the hydrographic and the high-resolution ADCP measurements enable a

qualitatively investigation of the circulation, the estimation of absolute transports remains problematic, because of the sensitivity of the integration to relatively small ADCP errors. Assuming spacing between stations of 56 km and a mean depth of (> 4000m) means an error in the referencing method of 2 cm s^{-1} translates into a 4.5 Sv error in the transport between one station pair.

5. Conclusions

Two consecutive surveys conducted during austral winter 2005 and austral summer 2005/2006 enables a hydrographic investigation of large parts of the southern limb of the Weddell Gyre. Although all presented measurements bear the character of a snapshot taken during summer and winter, a number of generally valid conclusions about the distribution, circulation and transports of the main water masses in the southern limb of the Weddell Gyre can be drawn.

An important result is that in both seasons two gateways are apparent, where warm deep water (WDW) masses, which are recognized by their temperature maximum, enter through the Lazarev Sea: (a) a probably topographically trapped west/southwest circulation around the northwestern edge of Maud Rise between 63° and 63.5°S with maximum velocities of about 10 cm s^{-1} and (b) Antarctic Coastal Current between 69° and 70°S, which is confined to the Antarctic continental shelf slope and is associated with maximum velocities of about 25 cm s^{-1}. Owing to a significant barotropic component, the derived flow field is essentially columnar without any pronounced layer of no motion and shows that calculations based on the dynamic method underestimate the transport considerably. The net absolute volume transports across the 3°E transects result in an eastward flow of 23.8 ± 19.9 Sv (austral summer) and 93.6 ± 20.1 Sv (austral winter). The major contributions to the net absolute transport stem from the

Maud Rise Jet, which accounts for 14.0 ± 5.1 Sv and 17.5 ± 5.2 Sv, and from the AntCC, which accounts for 7.8 ± 2.8 Sv and 13.5 ± 2.5 Sv during the summer and the winter survey, respectively.

Acknowledgements

This work forms part of the joint project LAKRIS (Lazarev Sea Krill Study) funded by the German Federal Ministry of Education and Research (Bundesministerium für Bildung und Forschung, BMBF). Harald Rohr and Timo Witte contributed substantially to the collection of the hydrographic dataset. We gratefully acknowledge the support provided by the captain, officers and crew of the R/V Polarstern.

Table 1. Summary of cruise dates

Cruise	Objective	Start	End	No. CTD stations	Cruise report
ANT-XXIII/2	Summer 2005/2006 survey	11/19/2005	01/12/06	87	Strass (2007)
ANT-XXIII/6	Winter 2006 survey	06/17/2006	08/21/06	90	Bathmann (2009)

Table 2. Main water masses of the Lazarev Sea

Acronym	Definitions
AASW	$S < 34.6$
WDW	$S > 34.6$, $\Theta > 0.0°C$
WSDW	$S > 34.64$, $-0.7°C < \Theta < 0.0°C$
WSBW	$S > 34.6$, $\Theta < -0.7°C$

AASW = Antarctic Surface Water, WDW = Warm Deep Water, WSDW = Weddell Sea Deep Water and WSBW = Weddell Sea Bottom Water.

Table 3. Geostrophic and ADCP-corrected zonal volume transports across 3°E (Austral summer). All values are in 10^6 m^3 s^{-1}, positive eastward. ADCP-corrected zonal transports are given, with the standard error. The transport has also been calculated for the main water masses.

Latitude	M_{Geo}	M_{Abs}	M_{AASW}	M_{WDW}	M_{WSDW}	M_{WSBW}
-60.2323	0.0	2.4 ± 6.0	0.1 ± 0.1	0.5 ± 1.2	1.2 ± 3.1	0.7 ± 1.6
-60.7424	0.5	1.4 ± 6.4	0.0 ± 0.2	0.4 ± 1.2	0.8 ± 3.3	0.3 ± 1.7
-61.2504	0.4	1.9 ± 6.0	0.1 ± 0.2	0.4 ± 1.0	0.9 ± 3.1	0.4 ± 1.7
-61.7359	-3.3	-5.4 ± 5.8	-0.3 ± 0.2	-1.5 ± 1.1	-3.0 ± 3.1	-0.6 ± 1.5
-62.2402	-2.7	-6.2 ± 6.4	-0.3 ± 0.2	-1.9 ± 1.3	-3.1 ± 3.5	-0.8 ± 1.4
-62.7542	2.5	1.9 ± 6.0	0.2 ± 0.2	0.9 ± 1.3	0.9 ± 3.2	-0.1 ± 1.3
-63.2436	-13.0	-14.0 ± 5.1	-0.8 ± 0.2	-6.3 ± 1.5	-6.9 ± 3.3	-0.0 ± 0.1
-63.7421	1.8	-10.3 ± 3.2	-0.4 ± 0.2	-5.1 ± 1.7	-4.8 ± 1.3	n. a.
-64.2492	0.6	1.9 ± 2.3	0.2 ± 0.2	1.3 ± 1.5	0.4 ± 0.7	n. a.
-64.7475	-0.3	0.5 ± 2.3	0.0 ± 0.2	0.3 ± 1.4	0.2 ± 0.8	n. a.
-65.2475	-0.1	2.7 ± 2.7	0.1 ± 0.1	1.4 ± 1.5	1.1 ± 1.0	n. a.
-65.7504	-0.5	1.3 ± 2.9	0.0 ± 0.2	0.6 ± 1.6	0.6 ± 1.2	n. a.
-66.2528	-0.2	2.8 ± 3.9	0.1 ± 0.2	1.1 ± 1.6	1.6 ± 2.1	n. a.
-66.7530	0.5	1.4 ± 3.6	0.1 ± 0.2	0.6 ± 1.6	0.7 ± 1.8	n. a.
-67.2519	-1.9	1.4 ± 3.6	0.0 ± 0.2	0.4 ± 1.7	1.0 ± 1.7	n. a.
-67.7303	0.2	3.4 ± 4.7	0.1 ± 0.1	1.2 ± 1.6	2.2 ± 2.9	n. a.
-68.2321	-1.6	-3.1 ± 5.1	-0.1 ± 0.2	-1.5 ± 2.0	-1.4 ± 2.9	n. a.
-68.7267	-0.7	-0.1 ± 3.8	-0.0 ± 0.1	-0.1 ± 1.7	0.0 ± 2.0	n. a.
-69.2234	-2.0	-6.4 ± 2.8	-1.6 ± 0.4	-3.9 ± 1.8	-0.9 ± 0.5	n. a.
-69.7441	-0.3	-1.4 ± 0.5	-1.4 ± 0.5	n. a.	n. a.	n. a.
Netto:	-20.1	-23.8 ± 19.9	-3.9 ± 1.0	-11.3 ± 6.6	-8.5 ± 10.5	-0.2 ± 3.8

Table 4. Geostrophic and ADCP-corrected zonal volume transports across 3°E (Austral winter). All values are in 10^6 m^3 s^{-1}, positive eastward. ADCP-corrected zonal transports are given, with the standard error. The transport has also been calculated for the main water masses.

Latitude	M_{Geo} [Sv]	M_{Abs} [Sv]	M_{AASW} [Sv]	M_{WDW} [Sv]	M_{WSDW} [Sv]	M_{WSBW} [Sv]
-60.1938	-1.8	6.4 ± 6.8	0.1 ± 0.2	0.9 ± 1.3	3.1 ± 3.5	2.3 ± 1.9
-60.7315	0.2	4.5 ± 6.6	0.1 ± 0.2	0.8 ± 1.3	2.4 ± 3.5	1.2 ± 1.7
-61.2434	-0.1	-9.0 ± 6.1	-0.3 ± 0.2	-1.7 ± 1.2	-4.8 ± 3.2	-2.3 ± 1.5
-61.7413	-0.6	-18.7 ± 5.9	-0.6 ± 0.2	-3.7 ± 1.2	-10.0 ± 3.2	-4.4 ± 1.4
-62.2338	-0.1	-15.8 ± 5.9	-0.4 ± 0.2	-3.4 ± 1.2	-8.4 ± 3.2	-3.6 ± 1.4
-62.7353	-1.0	-13.1 ± 6.2	-0.4 ± 0.2	-2.7 ± 1.3	-7.1 ± 3.3	-2.8 ± 1.4
-63.2338	-7.9	-17.5 ± 5.2	-0.7 ± 0.2	-6.3 ± 1.4	-9.8 ± 3.3	-0.6 ± 0.3
-63.7400	1.0	-5.2 ± 3.3	-0.2 ± 0.2	-2.4 ± 1.7	-2.6 ± 1.4	n. a.
-64.2695	0.5	-0.3 ± 2.5	0.0 ± 0.2	-0.1 ± 1.5	-0.2 ± 0.8	n. a.
-64.7884	-0.3	-0.5 ± 1.8	-0.1 ± 0.2	-0.4 ± 1.4	-0.0 ± 0.3	n. a.
-65.2750	-0.4	-0.4 ± 1.6	-0.0 ± 0.1	-0.3 ± 1.4	-0.0 ± 0.1	n. a.
-65.7613	-0.4	0.6 ± 3.0	-0.0 ± 0.1	0.3 ± 1.6	0.3 ± 1.2	n. a.
-66.2537	-0.2	-4.7 ± 3.5	-0.2 ± 0.1	-2.2 ± 1.6	-2.3 ± 1.7	n. a.
-66.7408	1.0	1.2 ± 3.6	0.1 ± 0.2	0.6 ± 1.7	0.5 ± 1.8	n. a.
-67.2219	-2.2	2.1 ± 3.4	0.0 ± 0.2	0.7 ± 1.6	1.4 ± 1.6	n. a.
-67.7040	-0.4	0.1 ± 5.1	-0.0 ± 0.2	-0.1 ± 1.8	0.2 ± 3.1	n. a.
-68.2458	-1.2	-6.4 ± 5.4	-0.2 ± 0.2	-2.7 ± 2.2	-3.4 ± 3.1	n. a.
-68.7503	0.1	-3.4 ± 3.5	-0.1 ± 0.1	-1.3 ± 1.6	-2.0 ± 1.9	n. a.
-69.2412	-1.8	-8.4 ± 2.4	-1.9 ± 0.4	-6.4 ± 2.0	-0.1 ± 0.0	n. a.
-69.7594	-1.3	-5.1 ± 0.5	-5.1 ± 0.5	n. a.	n. a.	n.a.
Netto:	-17.0	-93.6 ± 20.1	-9.9 ± 1.0	-30.7 ± 6.8	-42.8 ± 10.6	-10.2 ± 3.8

References

Bagriantsev, N.V., Gordon, A.L., Huber, B.A., 1989. Weddell Gyre: temperature maximum stratum. Journal of Geophysical Research 94, 8331-8334.

Bathmann, U. (Ed.), 2008. The expedition ANTARKTIS-XXIII/6 of the research vessel "Polarstern" in 2006. Berichte zur Polarforschung, 580, 1-168.

Beckmann, A., Hellmer, H.H., Timmermann, R., 1999. A numerical model of the Weddell Sea: large-scale circulation and water mass distribution. Journal of Geophysical Research 104, 23375–23391.

Bersch, M., Becker, G.A., Frey, H., Koltermann, K.-P., 1992. Topographic effects of the Maud Rise on the stratification of the Weddell Gyre. Deep-Sea Research 39, 303-331.

Carmack, E.C., Foster, T.D., 1975. On the flow of water out of the Weddell Sea. Deep-Sea Research 22, 711-724.

Cisewski, B., Strass, V.H., Prandke, H., 2005. Upper-ocean vertical mixing in the Antarctic Polar Frontal Zone. Deep-Sea Research II 52, 1087–1108.

Cisewski, B., Strass, V.H., Losch, M., Prandke, H., 2008. Mixed layer analysis of a mesoscale eddy in the Antarctic Polar Front Zone. Journal Geophysical Research 113, C05017, doi:10.1029/2007JC004372.

Cokelet, E.D., Schall, M.L., Dougherty, D.M., 1996. ADCP-referenced geostrophic circulation in the Bering Sea Basin. Journal of Physical Oceanography 26, 1113-1128.

Deacon, G.E.R., 1979. The Weddell Gyre. Deep-Sea Research 26A, 981–995.

De Steur, L., Holland, D.M., Muench, R.D., McPhee, M.G., 2007. The warm-water "Halo" around Maud Rise: Properties, dynamics and Impact. Deep-Sea Research I 54, 871-896.

Fahrbach, E., Knoche, M., Rohardt, G., 1991. An estimate of water mass transformation in the southern Weddell Sea. Marine Chemistry 35, 25-44.

Fahrbach, E., Rohardt, G., Schröder, M., Strass, V., 1994. Transport and structure of the Weddell Gyre. Annales Geophysicae 12, 840-855.

Firing, E., 1991. Acoustic Doppler current profiling measurements and navigation, WOCE Hydrographic Program Office Report. WHPO 91-9, WOCE Report. 68/91, 24 pp.

Foster, E., Carmack, E., 1976. Temperature and salinity structure in the Weddell Sea. Journal of Physical Oceanography 6, 36-44.

Gordon, A.L., Martinson, D.G., Taylor, H.W., 1981. The wind-driven circulation in the Weddell-Enderby Basin. Deep-Sea Research 28A, 151-163.

Gordon, A.L., Huber, B.A., 1990. Southern Ocean Winter Mixed Layer. Journal of Geophysical Research 95, 11655-11672.

Gordon, A.L., Huber, B.A., 1995. Warm Weddell Deep Water west of Maud Rise. Journal of Geophysical Research 100, 13747-13753.

Gouretski, V.V., Danilov, A.I., 1993. Weddell Gyre: structure of the eastern boundary. Deep-Sea Research I 40, 561–582.

Jacobs, S.S., 1991. On the nature and significance of the Antarctic Slope Front. Marine Chemistry 35, 9-24.

Johns, E., Watts, D.R., Rossby, H.T., 1989. A Test of Geostrophy in the Gulf Stream. Journal of Geophysical Research 94, 3211-3222.

Joyce, T. M., 1989, On In Situ Calibration of Shipboard ADCPs, Journal of Atmospheric and Oceanic Technology, 6, 169-17.

Klatt, O., Fahrbach, E., Hoppema, M., Rohardt, G., 2005. The transport of the Weddell Gyre across the Prime Meridian. Deep-Sea Research II 52, 513-528.

McPhee, M.G., Ackley, S.F., Guest, P., Huber, B.A., Martinson, D.G., Morison, J.H., Muench, R.D., Padman, L., Stanton, T., 1996. The Antarctic flux zone experiment. Bulletin of the American Meteorological Society 77, 1221-1232.

Muench, R.D., Morison, J.H., Padman, L., Martinson, D., Schlosser, P., Huber, B., Hohmann, R., 2001. Maud Rise revisited. Journal of Geophysical Research 106, 2423–2440.

Núñez-Riboni, I., Fahrbach, E., 2009. Seasonal variability of the Antarctic Coastal Current and its driving mechanisms in the Weddell Sea. Deep Sea Research I 56, 1927-1941.

Orsi, A.H., Nowlin Jr., W.D., Whitworth III, T., 1993. On the circulation and stratification of the Weddell Gyre. Deep-Sea Research I 40, 169–203.

Orsi, A.H., Johnson G.C., Bullister, J.L., 1999. Circulation, mixing and production of Antarctic Bottom Water. Progress of Oceanography 43, 55-109.

Padman, L., Fricker, H.A., Coleman, R., Howard, S., Erofeeva, L., 2002. A new tide model for the Antarctic ice shelves and seas. Annals of Glaciology 34, 247-254.

Pickart, R. S., Lindstrom, S., 1994. A Comparison of Techniques for Referencing Geostrophic Velocities. Journal Atmospheric Oceanic Technology 11, 814-824

Pollard, R.T., Read, J., 1989, A method of calibrating ship-mounted acoustic Doppler profilers and the limitations of gyro compasses, Journal *of Atmospheric and* Oceanic Technology *6*, 859-865.

Pond, S., Pickard, G.L., 1983. Introductory Dynamical Oceanography 2nd Edition. Pergamon Press, Oxford, 329 pp.

Schröder, M., Fahrbach, E., 1999. On the structure and the transport of the eastern Weddell Gyre. Deep-Sea Research II 46, 501–527.

Sirevaag, A., McPhee, M.G, Morison, J.H., Shaw, W.J., Stanton, T.P., 2010. Wintertime mixed layer measurements at Maud Rise, Weddell Sea. Journal of Geophysical research 115, doi:10.1029/2008JC005141

Strass, V. (Ed.), 2007. The expedition ANTARKTIS-XXIII/2 of the research vessel "Polarstern" in 2005/2006. Berichte zur Polarforschung, 568, 1-138.

Whitworth III, T., Nowlin, W.D., 1987. Water masses and currents of the Southern Ocean at the Greenwich Meridian. Journal of Geophysical research 92, 6462-6476.

Figure captions:

Fig. 1. Bathymetric map of the Atlantic and Indic sectors of the Southern Ocean including the study area (a). Station map with locations of CTD-profiles in the Lazarev Sea measured from R.V. *Polarstern* during austral summer 2005/2006 (b), and during austral winter 2006 (c). The depth contours (in meters) are taken from the General Bathymetric Chart of the Oceans (GEBCO) bathymetry.

Fig. 2. Potential temperature versus salinity diagram for the 3°E transect from austral summer 2005/2006 (a) and austral winter 2006 (b). AASW = Antarctic Surface Water, WDW = Warm Deep Water, WSDW = Weddell Sea Deep Water and WSBW = Weddell Sea Bottom Water.

Fig. 3. Vertical distribution of potential temperature (a) and salinity (b) along 3°E carried out during R.V. *Polarstern* cruise ANT-XXIII/2 (dashed curve indicates MLD). Station numbers are marked at the top of the section.

Fig. 4. Vertical distribution of potential temperature (a) and salinity (b) along 3°E carried out during R.V. *Polarstern* cruise ANT-XXIII/6 (dashed curve indicates MLD). Station numbers are marked at the top of the section.

Fig. 5. Bathymetry and circulation in the LAKRIS study area during R.V. *Polarstern* cruise ANT-XXIII/2. Tide-corrected ADCP velocity vectors are spatially averaged over 150-200 m depth and 5 km alongtrack (a). Streamfunction based on tide-corrected ADCP velocity vectors, which are spatially averaged over 150-200 m depth and temporarily averaged for

periods of hydrographic station work (b). Horizontal distribution of the temperature maximum (c).

Fig. 6. Bathymetry and circulation in the LAKRIS study area during R.V. *Polarstern* cruise ANT-XXIII/6. Tide-corrected ADCP velocity vectors are spatially averaged over 150-200 m depth and 5 km alongtrack (a). Streamfunction based on tide-corrected ADCP velocity vectors, which are spatially averaged over 150-200 m depth and temporarily averaged for periods of hydrographic station work (b). Horizontal distribution of the temperature maximum (c).

Fig. 7. Geostrophic velocity section referenced to the deepest common level of each station pair along 3°E during R.V. *Polarstern* cruise ANT-XXIII/2 (a) and ANT-XXIII/6 (b). Isotachs are in cm s^{-1}, and positive normal velocities represent eastward flow.

Fig. 8. Geostrophic velocity section referenced to ADCP velocities along 3°E during R.V. *Polarstern* cruise ANT-XXIII/2 (a) and ANT-XXIII/6 (b). Isotachs are in cm s^{-1}, and positive normal velocities represent eastward flow.

Fig. 9. Meridional distribution of the vertically integrated volume transports in 10^6 m^3 s^{-1} for each station pair: (a) geostrophic transport (referenced to the deepest common level of each station pair), (b) ADCP-referenced geostrophic transport, ADCP-referenced water mass transports for : (c) AASW, (d) WDW, (e) WSDW and (f) WSBW. Error bars are based on standard deviations of the current speeds used in estimating the transports.

Fig. 10. Meridional distribution of vertically integrated volume transports in 10^6 m^3 s^{-1} for each station pair: (a) geostrophic transport (referenced to the deepest common level of each station pair), (b) ADCP-referenced geostrophic transport, ADCP-referenced water mass transports for : (c) AASW, (d) WDW, (e) WSDW and (f) WSBW. Error bars are based on standard deviations of the current speeds used in estimating the transports.

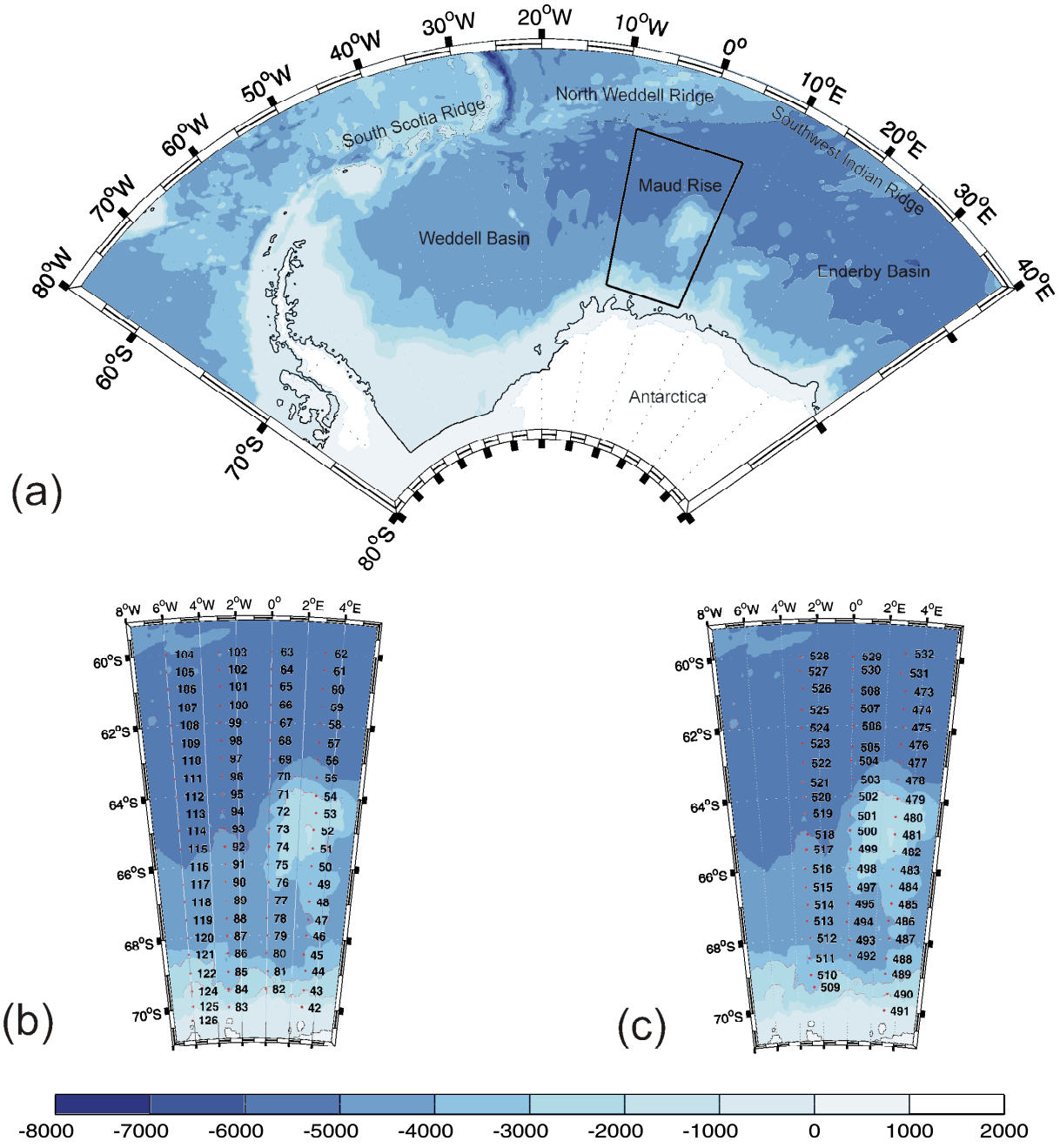
(a)
South Scotia Ridge
North Weddell Ridge
Southwest Indian Ridge
Maud Rise
Weddell Basin
Enderby Basin
Antarctica
(b)
(c)
-8000
-7000
-6000
-5000
-4000
-3000
-2000
-1000
0
1000
2000

Fig. 1

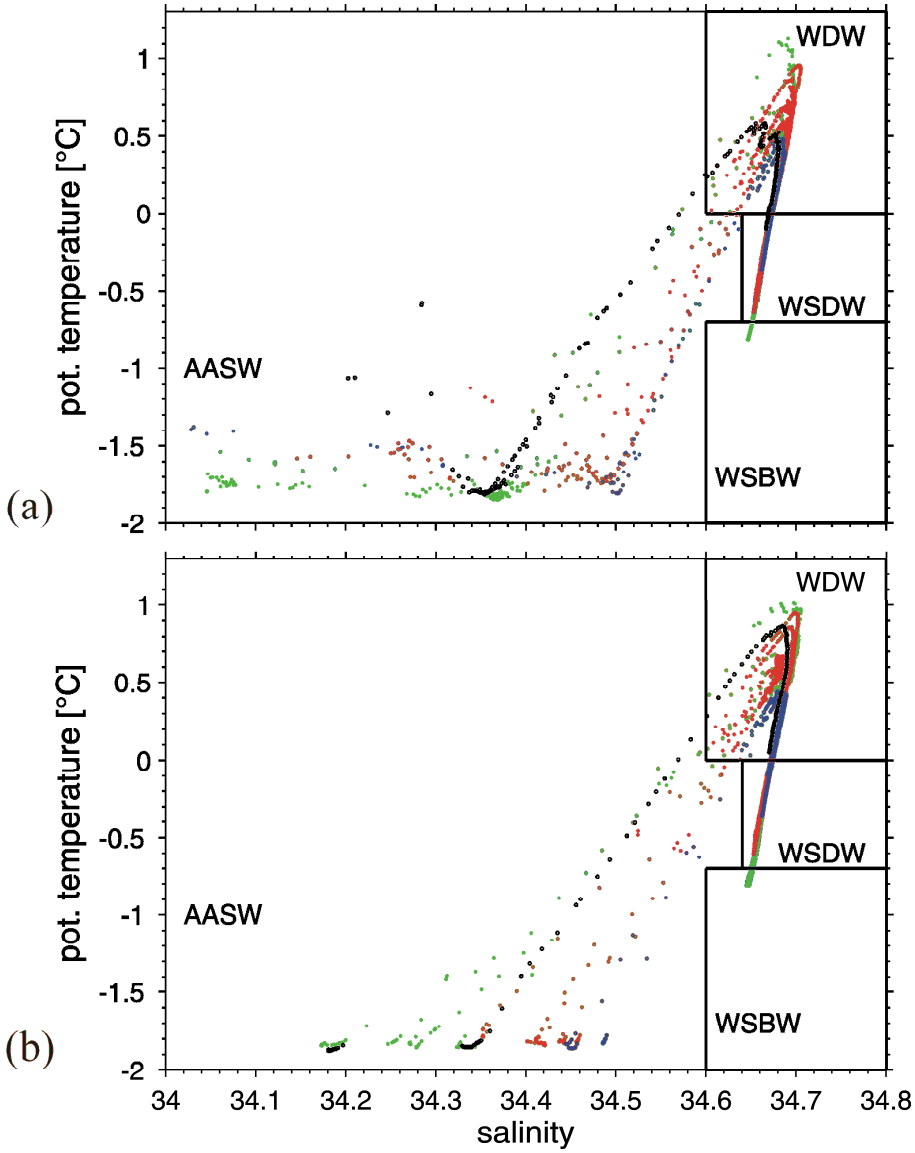
(a)
(b)
pot. temperature [°C]
salinity
WDW
WSDW
WSBW
AASW
1
0.5
0
-0.5
-1
-1.5
-2
34
34.1
34.2
34.3
34.4
34.5
34.6
34.7
34.8

Fig. 2

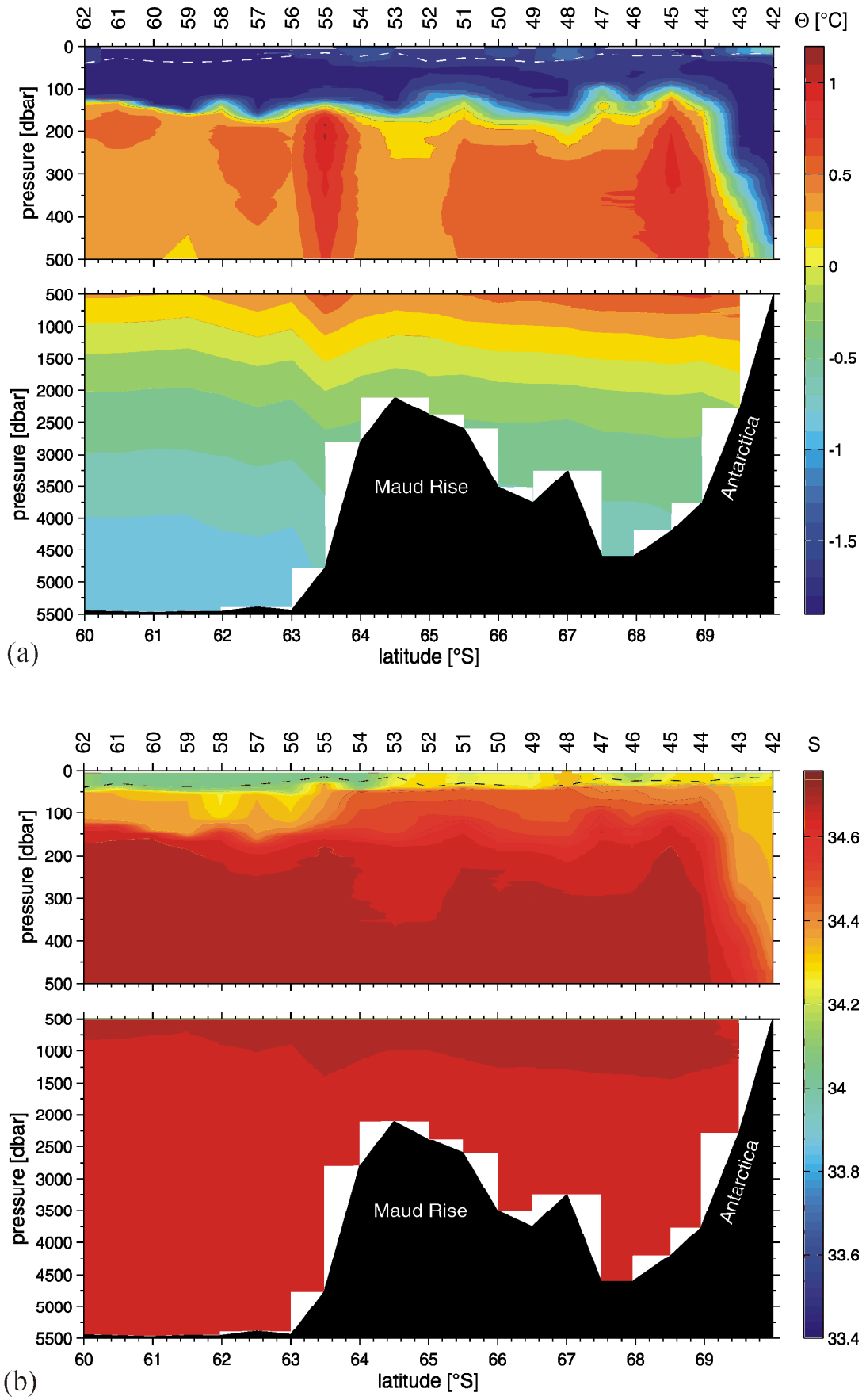
62 61 60 59 58 57 56 55 54 53 52 51 50 49 48 47 46 45 44 43 42
Θ [°C]
pressure [dbar]
0 100 200 300 400 500
1 0.5 0 -0.5 -1 -1.5
500 1000 1500 2000 2500 3000 3500 4000 4500 5000 5500
Maud Rise
Antarctica
60 61 62 63 64 65 66 67 68 69
latitude [°S]
(a)
S
34.6 34.4 34.2 34 33.8 33.6 33.4
(b)

Fig. 3

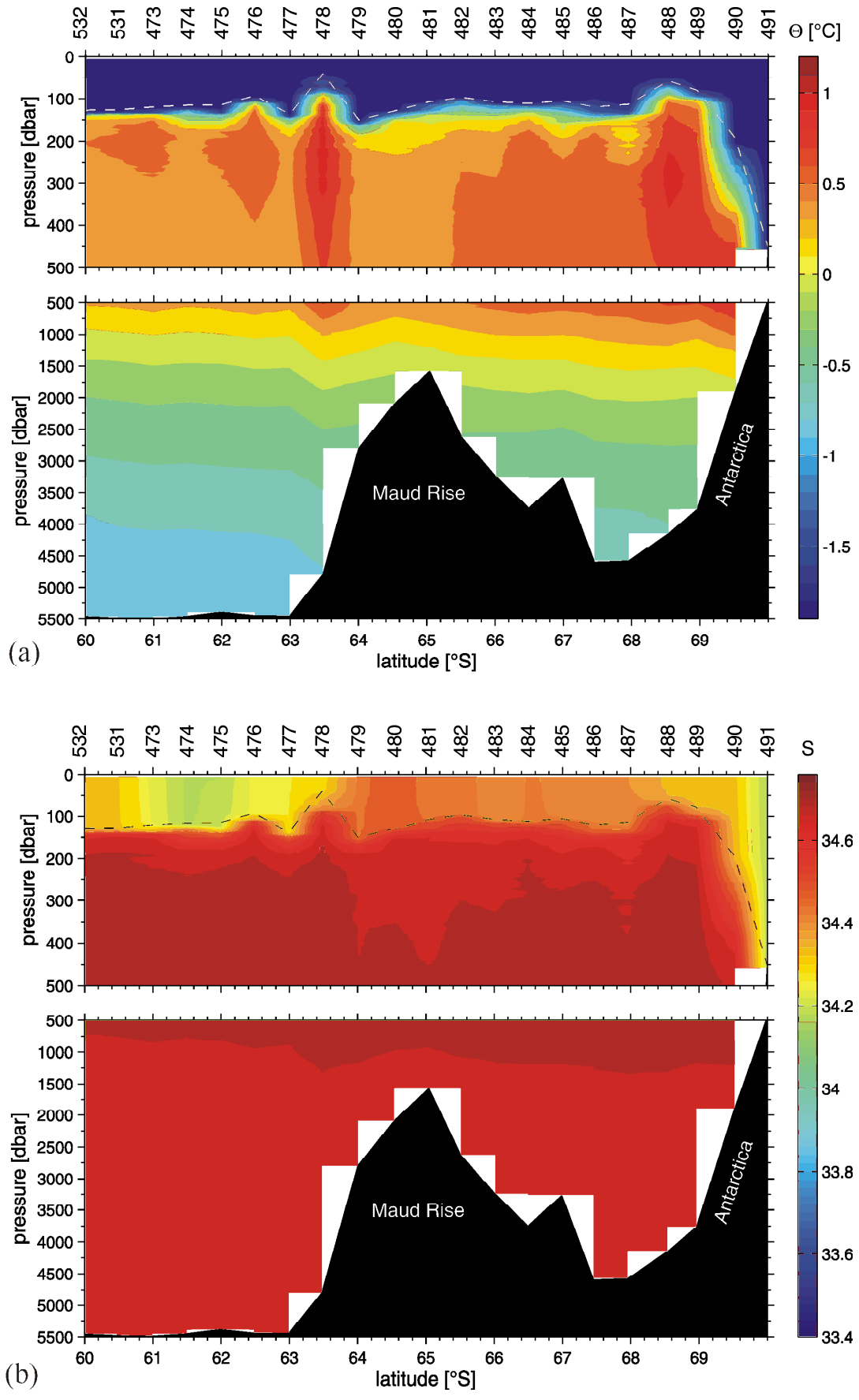
532 531 473 474 475 476 477 478 479 480 481 482 483 484 485 486 487 488 489 490 491
Θ [°C]
pressure [dbar]
0 100 200 300 400 500
1 0.5 0 -0.5 -1 -1.5
500 1000 1500 2000 2500 3000 3500 4000 4500 5000 5500
Maud Rise
Antarctica
60 61 62 63 64 65 66 67 68 69
latitude [°S]
(a)
S
34.6 34.4 34.2 34 33.8 33.6 33.4
(b)

Fig. 4

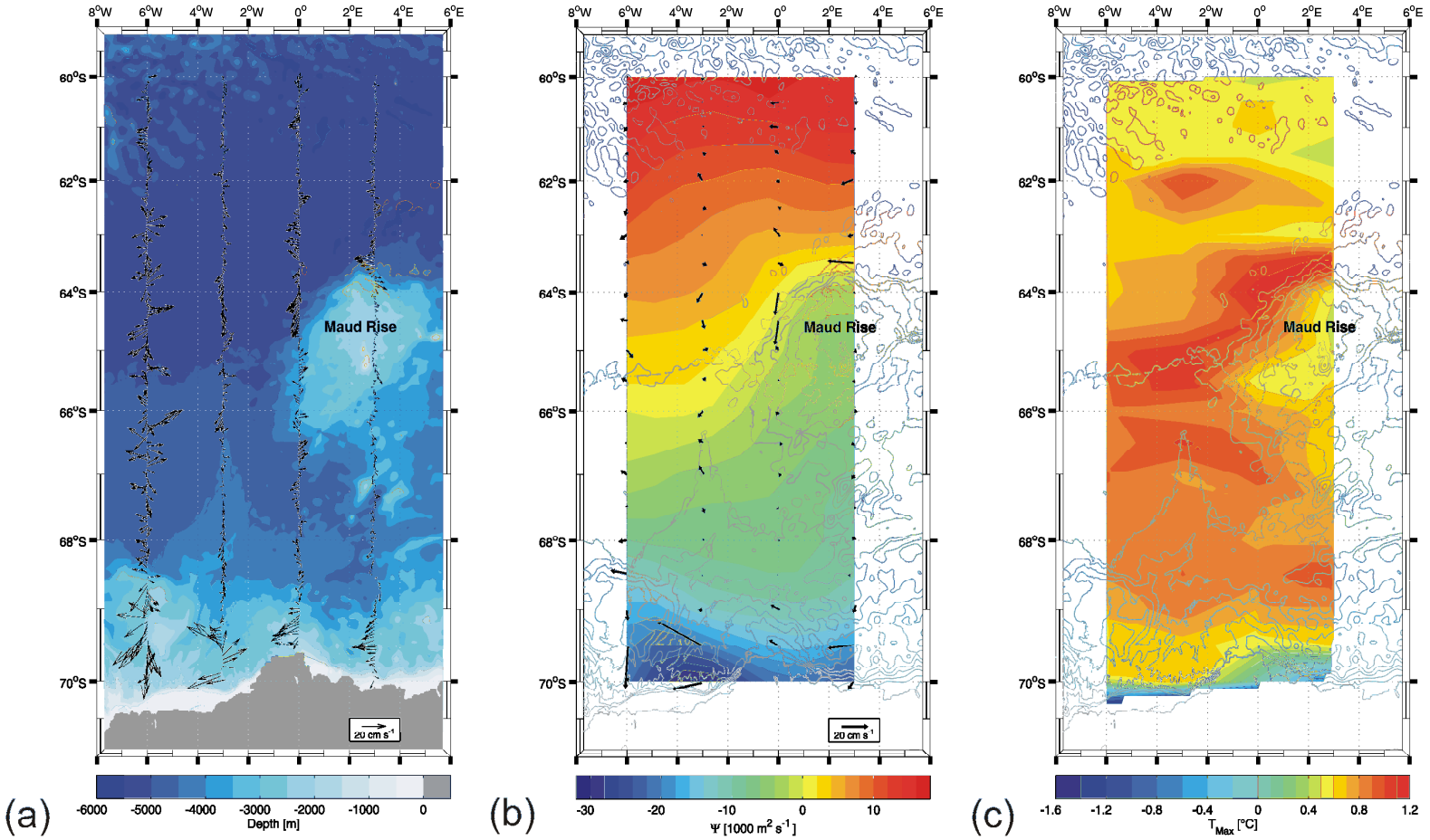
8°W
6°W
4°W
2°W
0°
2°E
4°E
6°E
60°S
62°S
64°S
66°S
68°S
70°S
Maud Rise
20 cm s⁻¹
(a)
-6000
-5000
-4000
-3000
-2000
-1000
0
Depth [m]
(b)
-30
-20
-10
0
10
Ψ [1000 m² s⁻¹]
(c)
-1.6
-1.2
-0.8
-0.4
0
0.4
0.8
1.2
T_Max [°C]

Fig. 5

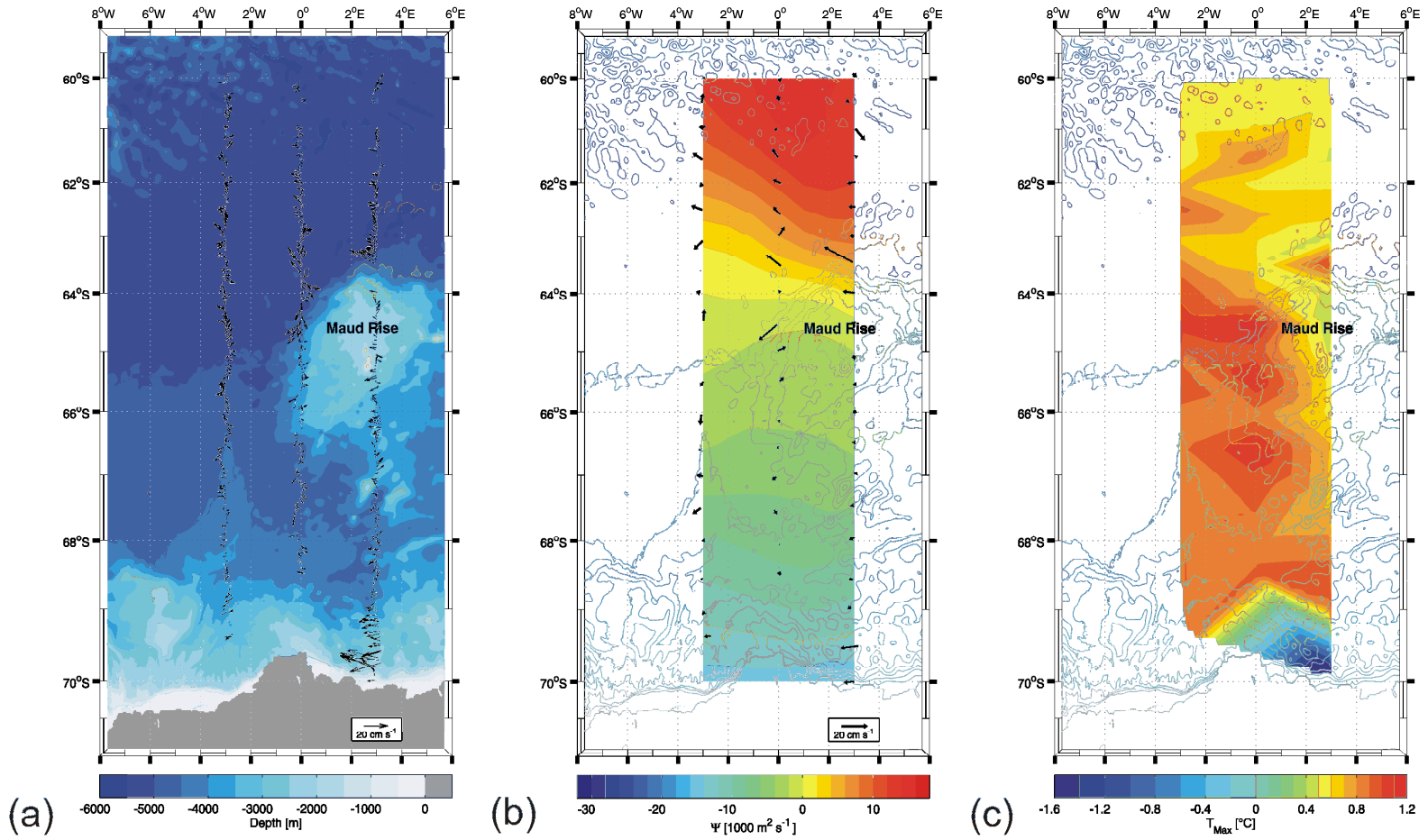
8°W
6°W
4°W
2°W
0°
2°E
4°E
6°E
60°S
62°S
64°S
66°S
68°S
70°S
Maud Rise
20 cm s⁻¹
(a)
-6000
-5000
-4000
-3000
-2000
-1000
0
Depth [m]
(b)
-30
-20
-10
0
10
Ψ [1000 m² s⁻¹]
(c)
-1.6
-1.2
-0.8
-0.4
0
0.4
0.8
1.2
T_Max [°C]

Fig. 6

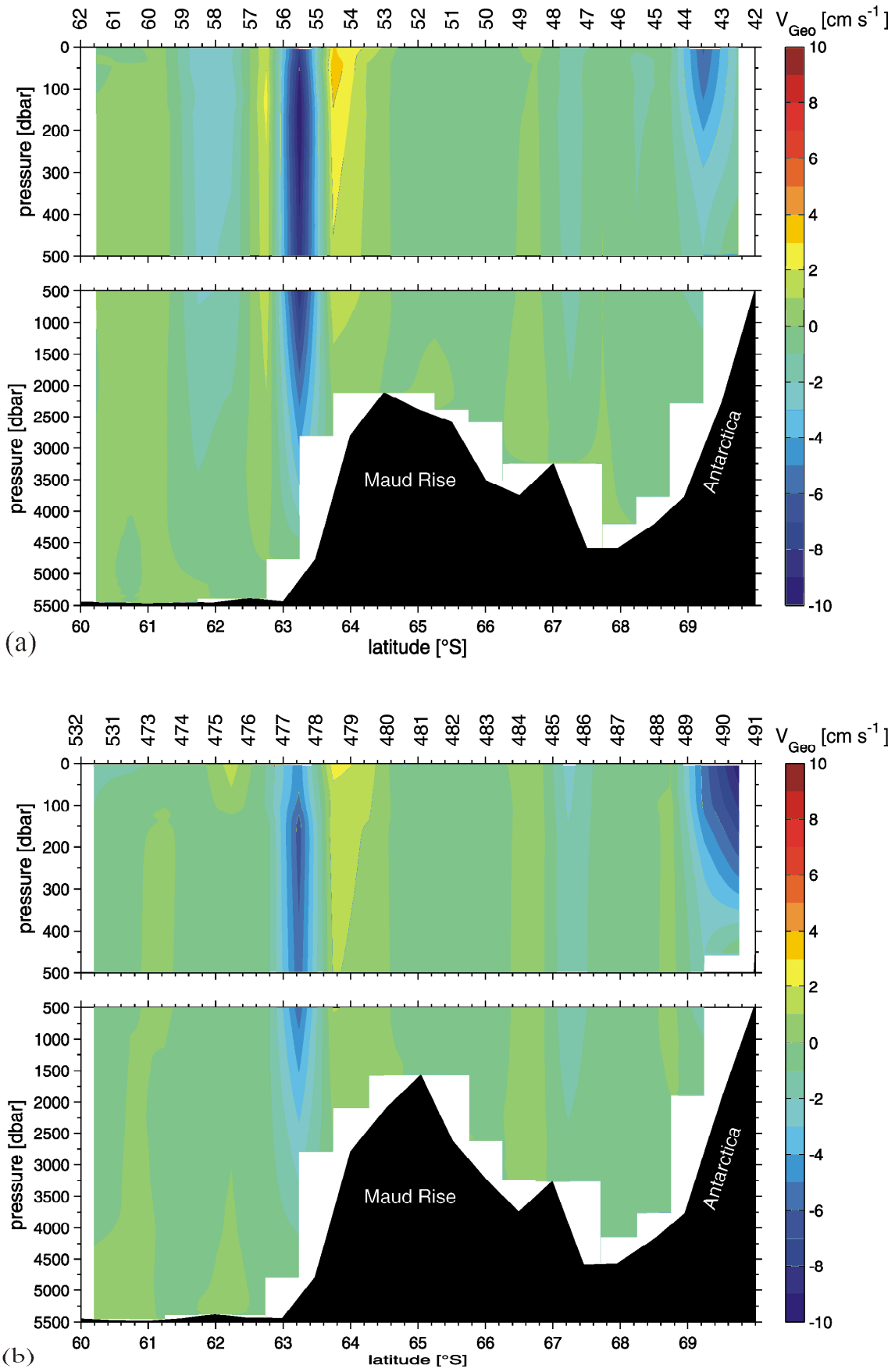

Fig. 7

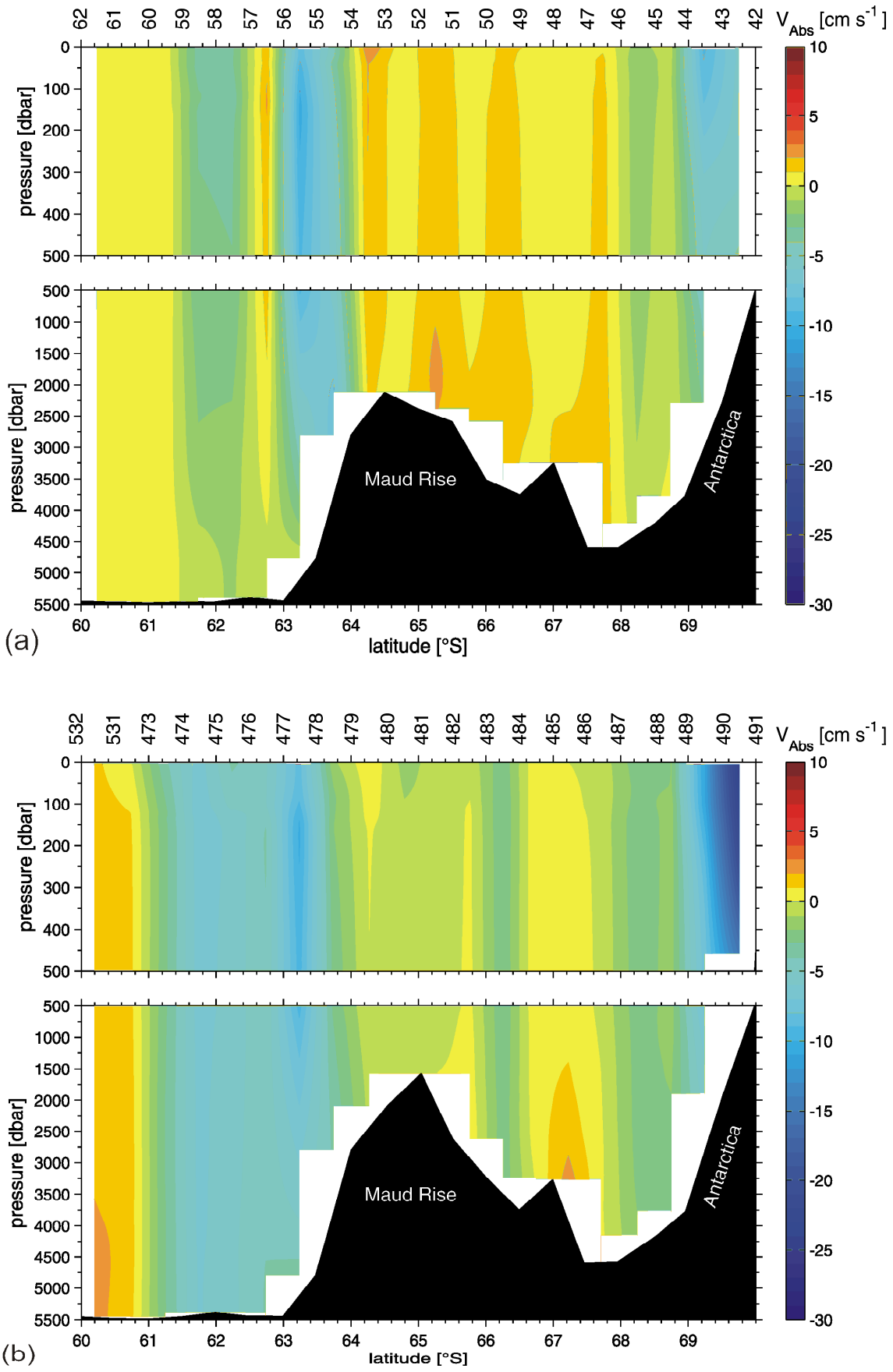

Fig. 8

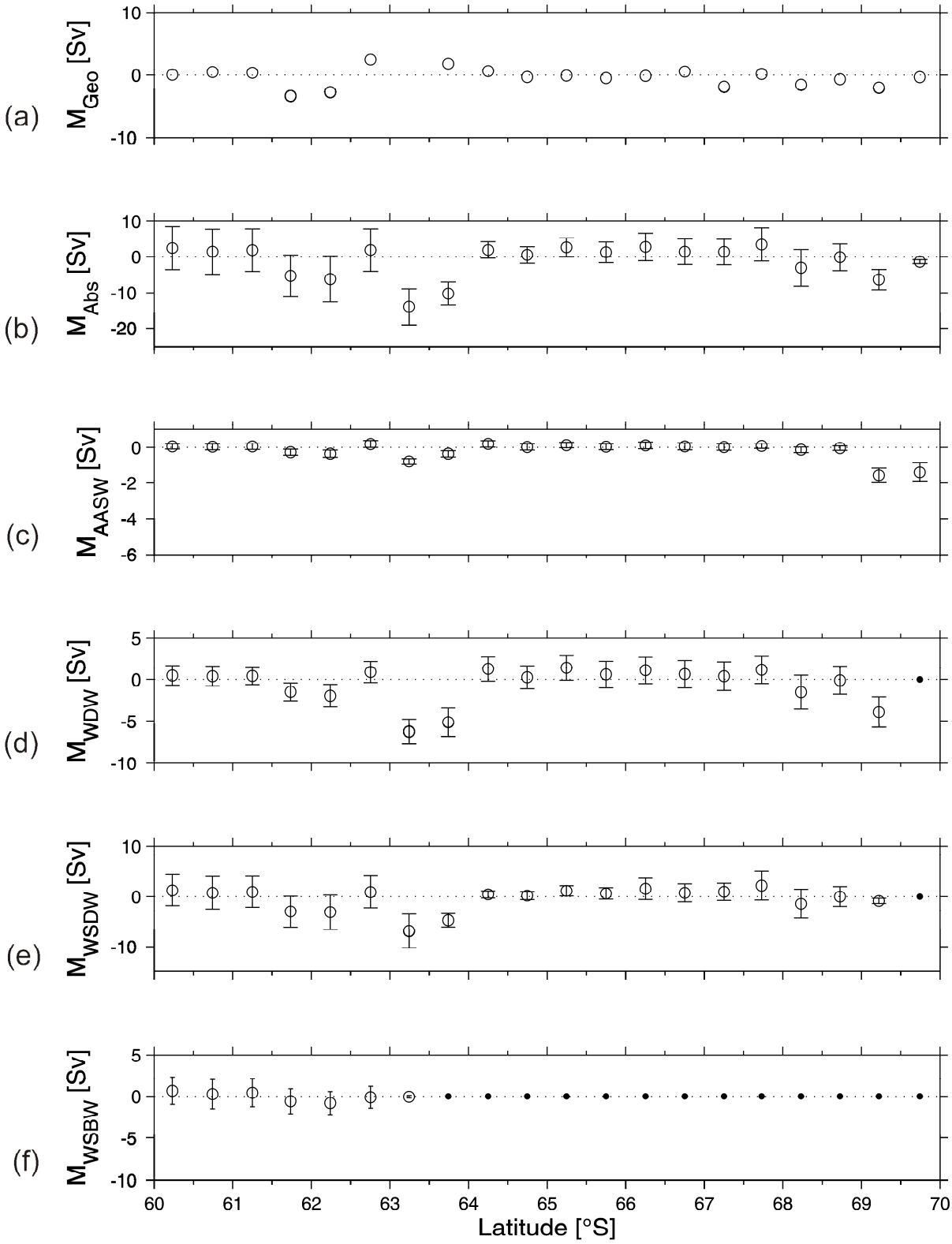
(a)
M_{Geo} [Sv]
10
0
-10
(b)
M_{Abs} [Sv]
10
0
-10
-20
(c)
M_{AASW} [Sv]
0
-2
-4
-6
(d)
M_{WDW} [Sv]
5
0
-5
-10
(e)
M_{WSDW} [Sv]
10
0
-10
(f)
M_{WSBW} [Sv]
5
0
-5
-10
60
61
62
63
64
65
66
67
68
69
70
Latitude [°S]

Fig. 9

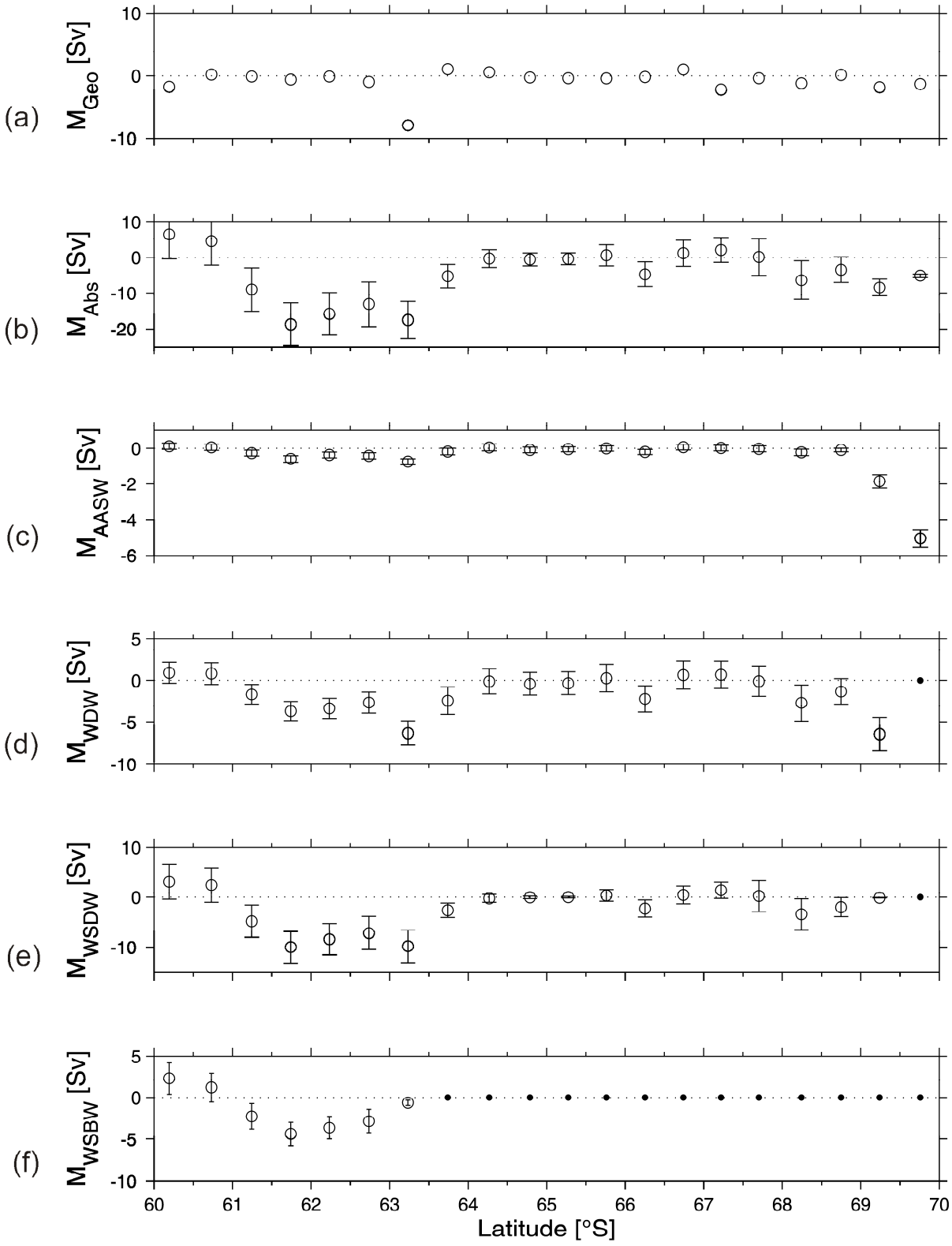
(a)
M_{Geo} [Sv]
10
0
-10
(b)
M_{Abs} [Sv]
10
0
-10
-20
(c)
M_{AASW} [Sv]
0
-2
-4
-6
(d)
M_{WDW} [Sv]
5
0
-5
-10
(e)
M_{WSDW} [Sv]
10
0
-10
(f)
M_{WSBW} [Sv]
5
0
-5
-10
60
61
62
63
64
65
66
67
68
69
70
Latitude [°S]

Fig. 10